

Dependence of the textural properties and surface species of ZnO photocatalytic materials on the type of precipitating agent used in the hydrothermal synthesis

I STAMBOLOVA^{1,*}, V BLASKOV¹, D STOYANOVA¹, I AVRAMOVA¹, L DIMITROV²,
K MILENOVA³, K BALASHEV⁴, S SIMEONOVA⁴, A TZONEV⁵, L ALEKSANDROV¹ and
A ELIYAS³

¹Institute of General and Inorganic Chemistry, Bulgarian Academy of Sciences, 1113 Sofia, Bulgaria

²Institute of Mineralogy and Crystallography ‘Academician I Kostov’, Bulgarian Academy of Sciences, 1113 Sofia, Bulgaria

³Institute of Catalysis, Bulgarian Academy of Sciences, 1113 Sofia, Bulgaria

⁴Faculty of Chemistry and Pharmacy, Sofia University, St. Kliment Ohridski, 1164 Sofia, Bulgaria

⁵Solid State Physics and Microelectronics Department, Faculty of Physics, Sofia University, St. Kliment Ohridski, 1164 Sofia, Bulgaria

*Author for correspondence (stambolova@yahoo.com)

Abstract. Three different precipitating agents (NaOH, NH₄(H)CO₃ and CO(NH₂)₂) have been applied for the hydrothermal synthesis of ZnO powder materials, aiming at obtaining various types of porosity and surface species on ZnO. The synthesis procedures were carried out in the presence and in the absence of tri-block copolymer Pluronic (P123, EO20PO70EO20). These materials were characterized by powder X-ray diffraction (PXRD), X-ray photoelectron spectroscopy (XPS), scanning electron microscopy (SEM)–energy-dispersive X-ray spectroscopy (EDX), BET method and TG–differential thermal analysis (DTA) method, and their photocatalytic activities were tested in the removal of azo dye Reactive Black 5 (RB5). The urea precipitant yields spongy-like surface forms and the greatest share of mesopores. It has the highest specific surface area, highest degree of crystallinity of wurtzite ZnO phase and largest content of surface OH groups in comparison with the other two precipitants. The zinc hydroxycarbonate intermediate phase is missing in the case of NaOH as precipitating agent; therefore, it manifests poorer textural characteristics. The morphology of P123-modified sample is different and consists of needle-shaped particles. The urea-precipitated samples display superior performance in the photocatalytic oxidation reaction, compared with the other precipitated samples. The other two precipitating agents are inferior in regard to their photocatalytic activity due to greater share of micropores (not well-illuminated inner surface) and different surface morphologies.

Keywords. Zinc oxide; hydrothermal synthesis; porosity; photocatalyst.

1. Introduction

Zinc oxide is a wide bandgap semiconductor (3.37 eV) with wurtzite crystalline structure possessing excellent features like electronic, optical, sensing and catalytic properties, which favor its numerous potential applications in various electronic, optoelectronic, sensor, energy storage and other devices [1]. Other ZnO applications and major uses of ZnO, particularly in the form of powder, are pigments [2], photocatalysts [3] and UV-light absorbers [4].

Photocatalytic oxidation, based on UV-light-irradiated semiconductors such as TiO₂, ZnO, WO₃, Fe₂O₃, etc., is a powerful process for discoloration of wastewaters, since the chromophore groups can be broken down, leading to their degradation and complete mineralization. Among them, ZnO is a suitable inexpensive and non-toxic compound having high photocatalytic efficiency for detoxification of organic dyes [4, 5]. Many expensive ZnO synthesis methods, such as mechanical milling [6], thermal evaporation of zinc metal [7] or decomposition of zinc-containing salts [8], have been applied. The wet chemical methods have the potential advantage of large-scale preparations for high-technology applications. Among the ZnO powders preparation techniques, the hydrothermal method is a low-cost and fast synthesis method, offering potential capability to obtain lowly aggregated ZnO structures with different morphologies, narrow grains size distributions and high-degree purity without any heat treatment at high temperature [9].

Some authors have applied hydrothermal preparation of ZnO by precipitation with nitrogen-containing compounds such as urea (U) [10,11] and ammonium carbonate (HC) [12,13], which are cheap, safe and highly water-soluble compounds,

therefore easily to be separated and removed. The application of these precipitants is attractive repeatable and easily controlled strategy for the synthesis of nanosized ZnO particles.

Surfactant-assisted hydrothermal methods have been recently applied to the synthesis of porous ZnO with high degree of crystallinity and chemical and thermal stability. Many types of surfactants have been reported, including polyethylene glycol (PEG) [14] and cetyltrimethyl ammonium bromide (CTAB) [15]. Recently we have prepared successfully ZnO powder photocatalysts by P123-assisted precipitation of zinc acetate with NaOH, followed by hydrothermal treatment [16,17].

The aim of this paper was to study the dependence of the textural properties, surface species and phase composition on the type of precipitating agent used in the hydrothermal synthesis of ZnO photocatalytic materials.

2. Experimental

2.1 Preparation of the samples

Three different synthesis procedures were applied.

- (i) The first synthesis step is dissolving 2.2g zinc acetate in 100ml of deionized water. Sodium hydroxide aqueous solution was added dropwise to the acetate solution until pH=12–13 was reached. Then 4g of tri-block copolymer Pluronic (P123, EO20PO70EO20) was added to this solution under magnetic stirring. The resulting mixture was transferred into an autoclave maintained at 140°C for 12h. The resulting samples are denoted as N1. Reference sample was obtained from the solution without any P123 under the same preparation conditions and denoted as N0.
- (ii) Aqueous HC solution (0.5M) was added dropwise to 0.2M aqueous (2.2g in 100ml water) zinc acetate solution until pH=7 was reached. Then 4g P123 was added to the acetate solution. The resulting mixture was transferred into an autoclave maintained at 140°C for 12h. The resulting samples are denoted as C1. Reference sample was obtained from the solution without any P123 under the same preparation conditions and denoted as C0.
- (iii) Urea aqueous solution (0.6M) was added dropwise to 0.2M zinc acetate solution. The pH of solution was adjusted to 7 using ammonium hydroxide. Then 4g of P123 was added to this solution. The resulting mixture was transferred into an autoclave maintained at 90°C for 12h. The resulting samples are denoted as U1. Reference sample was obtained without any P123 under the same preparation conditions and denoted as U0.

2.2 Characterization of the samples

The X-ray diffraction (XRD) patterns were recorded on a Bruker D2 Phaser diffractometer within the range of 2θ values between 25° and 75° using Cu K α radiation ($\lambda = 0.154056\text{nm}$) at 40kV. The express BET method has been applied to measure the specific surface area, based on low temperature adsorption of nitrogen. The relative error of the method is about 8%. The specific surface area and the pore size distribution measurements were accomplished on an automated apparatus NOVA Win—CFR Quanta chrom — Gas Sorption System. The calculation of the surface area was done using the BET equation, whereupon the pore size distribution and the average pore diameter were evaluated by the DFT method assuming a cylindrical model of the pores. The total pore volume was estimated in accordance with the rule of Gurvich at relative pressure of 0.96.

The X-ray photoelectron spectroscopy (XPS) analyses were performed on a Kratos AXIS Supra instrument with a monochromatic Al X-ray source. Each analysis started with a survey scan from 0 to 1200eV at a pass energy of 160eV, and steps of 1eV with 1 sweep. For the high-resolution analysis the number of sweeps was increased, and the pass energy was lowered down to 20eV at steps of 100meV. The XPS method was used for the investigation of the surface of ZnO powders synthesized by different methods. The binding energy of C1s photoelectron line at 285.0eV belonging to the adventitious carbon was used for calibration. The C1s, O1s and Zn2p photoelectron lines were recorded and the obtained spectra were analyzed. No additional peak corresponding to any impurities in the sample, other than Zn and O, is observed.

The morphology of the powder samples has been analyzed using a combined scanning electron microscopy (SEM) focused ion beam system LYRA XMU (Tescan). The scanning electron images have been obtained at 30 kV accelerating voltage, using a secondary electron (SE) detector, which gives information about morphology and surface topography of the sample. The samples were coated with a thin layer of carbon and gold for better conductivity prior to the investigation. Energy-dispersive X-ray spectroscopy (EDX) analysis was performed in order to obtain information about elemental composition. EDX spectra have been collected using the point analysis method, which gives precise information at a single point. The X-ray detector used is a Quantax 200 BRUKER.

The differential thermal analysis (DTA) has been accomplished on a combined DTA–TG apparatus LABSYSEVO 1600 manufactured by the SETARAM Company (France). Synthetic air was used as the carrier gas, with flow rate of 20ml min⁻¹. The rate of heating was 10K min⁻¹ upto 350°C. A corundum crucible and a Pt/Pt–Rh thermocouple have been used.

The diffuse reflectance (DR) UV–Vis spectra were recorded with a Thermo Evolution 300 UV–visible spectrophotometer equipped with a Praying Mantis device. The spectra of Spectralon were used for background calibration (Spectralon is a fluoropolymer that has the highest DR of any known material or coating over the ultraviolet, visible and near-infrared regions of the spectrum).

2.3 Testing of the photocatalytic activity

The photocatalytic oxidative discoloration of Reactive Black 5 (RB5) azo dye was evaluated using RB5 aqueous solution of initial concentrations 20 and 40ppm. The photocatalytic activity measurements were conducted under polychromatic UV-A lamp illumination (power 18W, light intensity $5 \times 10^{-5} \text{ Wcm}^{-2}$) with maximum emission at wavelength 365nm. The reactor contained 20 or 40ppm water solution (150ml) of RB5. The course of the oxidative discoloration reaction was monitored by a UV–visible absorbance spectrophotometer UV-1600PC within the wavelength range 200–800nm. The samples were equilibrated in the dark (reaching adsorption-desorption equilibrium) for about 30 min before switching on the irradiation. The photocatalytic efficiencies of the samples were evaluated in the reaction of RB5 oxidative discoloration and the results are plotted based on the equation

$$C/C_0 = f(t), \quad (1)$$

where C_0 is the initial concentration of the dye and C is the concentration of the dye after irradiation after a certain time interval t .

3. Results and discussion

3.1 Structure and morphology of the samples

The XRD patterns of both samples N0 and N1 revealed narrow and sharp diffraction peaks, which proved the existence of well-crystallized wurtzite polycrystalline phase. The phase corresponds well to hexagonal type of structure characteristic of ZnO (JCPDS 36-1451; figure 1). It can be seen that the sample obtained from polymer-modified HT process possesses higher degree of crystallinity than that of the sample without polymer addition. The average crystallite sizes of the samples, evaluated by the Scherrer formula, are 21 and 7nm for N0 and N1 samples, respectively.

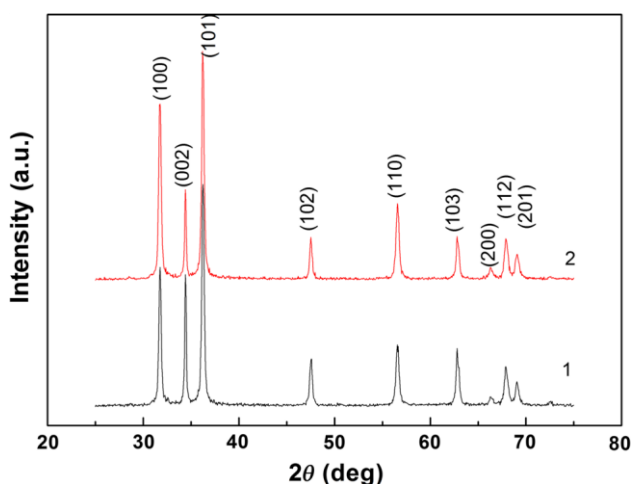


Figure 1. XRD patterns of (1) sample N0 and (2) sample N1.

Figure 2 presents the X-ray diffractograms of the C0 sample. The diffractogram after hydrothermal treatment at 140°C reveals peaks corresponding to zinc hydroxycarbonate $Zn_5(CO_3)_2(OH)_6$ that are consistent with the values of the database JCPDS 19-1458 (pattern 1). This intermediate compound was reported by Chen *et al* [11] after direct precipitation of zinc nitrate with ammonium carbonate. After thermal treatment of zinc hydroxycarbonate $Zn_5(CO_3)_2(OH)_6$ at 170°C it is not completely decomposed and only a fraction of it is transformed into wurtzite ZnO (figure 2—pattern 2). At 200°C the formation of well-crystallized wurtzite phase is completed. The sample C1, obtained from Pluronic-assisted HT process and annealed at 170°C, contains only zinc hydroxycarbonate phase, which is not so well crystallized compared with the C0 sample (figure 3). The wurtzite phase is formed after treatment at 200°C. The average crystallite sizes of the samples, evaluated by the Scherrer formula, are 10nm for both C0 and C1 samples.

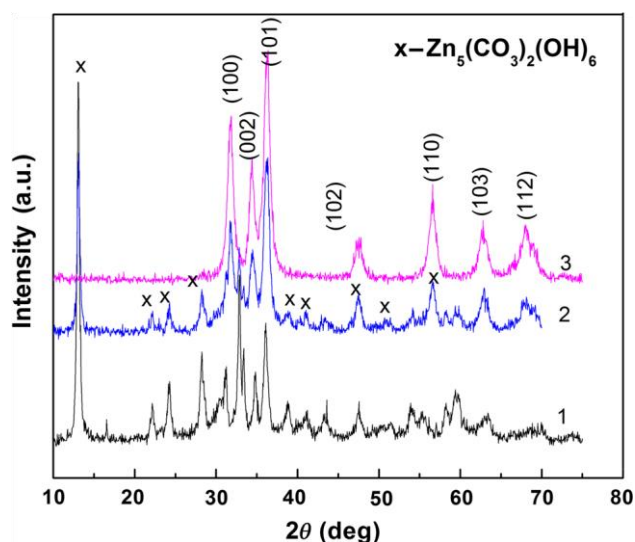


Figure 2. XRD patterns of C0 sample (1) after HT, (2) after treatment at 170°C and (3) after treatment at 200°C.

In the case of urea-assisted HT process the sample U0 possesses poorly crystallized zinc hydroxycarbonate (figure 4). It decomposes completely into ZnO wurtzite phase at 170°C with two predominant peaks, which correspond to (100) and (101) planes. This is in contrast with the randomly oriented zinc oxide, obtained in the cases of NaOH- and NH_4HCO_3 assisted HT procedures. A similar X-ray diffractogram is registered with the U1 sample. The average crystallite sizes of the samples, evaluated by the Scherrer formula, are 17 and 12 nm for U0 and U1 samples, respectively. It should be noted that the sample obtained from polymer-modified HT process possesses lower degree of crystallinity than that of samples without polymer addition, in contrast with the samples C0 and C1. It is also notable that in the case of urea precipitant the powders obtained exhibit higher degree of crystallization. This can be explained by the supersaturated nucleation, which may accelerate crystallization. This effect of urea precipitant is in accordance to the results published in [18].

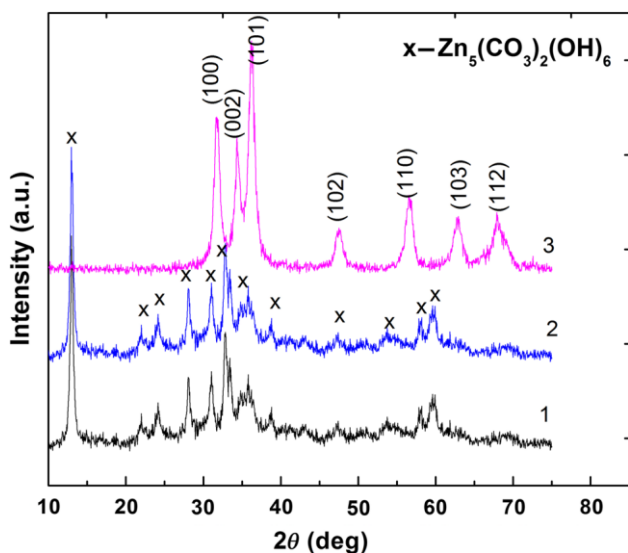


Figure 3. XRD patterns of C1 sample (1) after HT, (2) after treatment at 170°C and (3) after treatment at 200°C .

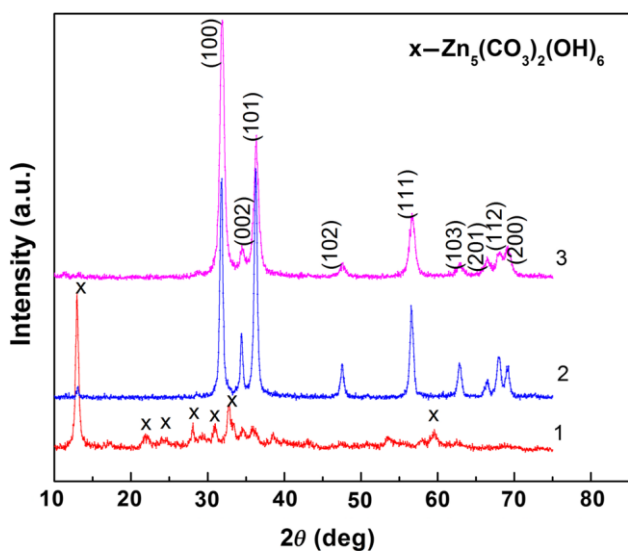


Figure 4. XRD of U0 sample (1) after HT, (2) after treatment at 170°C and (3) U1 sample after treatment at 170°C .

The adsorption–desorption isotherms (not shown here) of both N0 and N1 samples can be classified as type IV of the IUPAC nomenclature, which reveal the dominating presence of mesopores. The hysteresis loop could be interpreted as one belonging to the type H3. An almost horizontal section is observed, whereupon the hysteresis loop is shifted towards higher relative pressures (P/P_0 approximately 1), which implies the presence of cylindrical pores. A similar behavior was observed with the ZnO particles [19]. The pore size distributions of the samples are shown in figure 5.

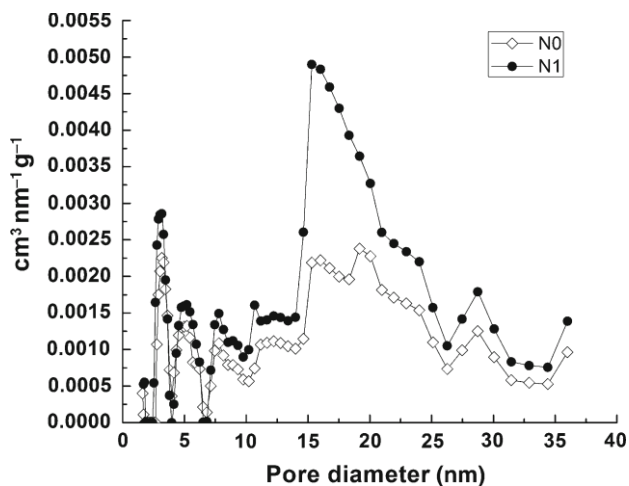


Figure 5. Pore size distributions of N0 and N1 samples.

The BET surface areas (S) are as follows: $S_{N0} = 10\text{m}^2\text{g}^{-1}$ and $S_{N1} = 13\text{m}^2\text{g}^{-1}$, while the average pore diameters are 8.4 and 9.2nm for the N0 and N1 samples, respectively. The polymer modification of the zinc precursor solution increases the relative share of the mesopores at the expense of the share of micropores.

The powder obtained from NH_4HCO_3 -assisted HT procedure at 140°C exhibits one narrow peak corresponding to some quantity of micropores up to 20nm and a broad peak appearing in the pore size region from 20 to 50nm. It has to be noted that the sample C0 possesses larger pore volume and greater average pore diameter ($0.09\text{cm}^3\text{g}^{-1}$ and 15nm, respectively) than those of samples obtained from sodium hydroxide (N). The C1 sample does not reveal any substantial difference in the pore size distribution, compared to the C0 sample.

The pore size distributions of the specimens prepared by HT procedure with urea as precipitant are shown in figure 6. They follow a bimodal pattern. One pore group is representative of micropores, whose size is less than 10 nm, and the other pore group consists of bigger mesopores, whose size is in the range 15–50nm. It has to be noted that the U0 sample possesses increased share of mesopores and macropores in comparison with the U1 sample. Similar distributions of pore size have been obtained by Miao *et al* [20] for ZnO powders produced hydrothermally from zinc acetate and urea.

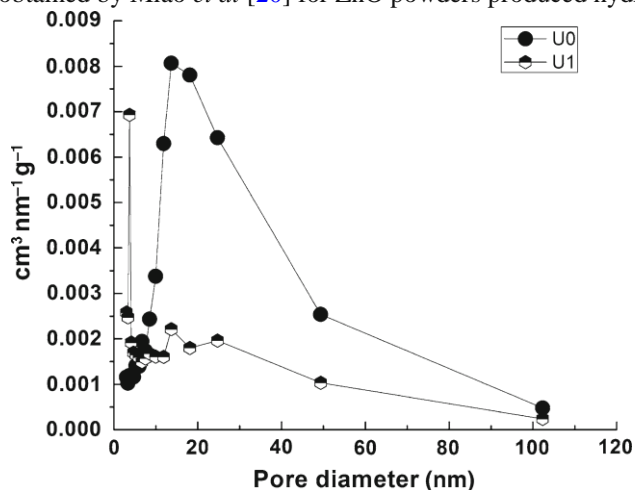


Figure 6. Pore size distributions of the U0 and U1 samples.

Figure 7 summarizes the data on the specific surface areas, average pore volumes and average pore sizes for all HT samples. It should be noted that the samples U0 and C0 possess higher specific surface areas (lower precipitation rate at $\text{pH}=7$), compared with the N0 sample. The area decrease in the U1 and in the C1 sample can be explained by polymer blocking of the pores.

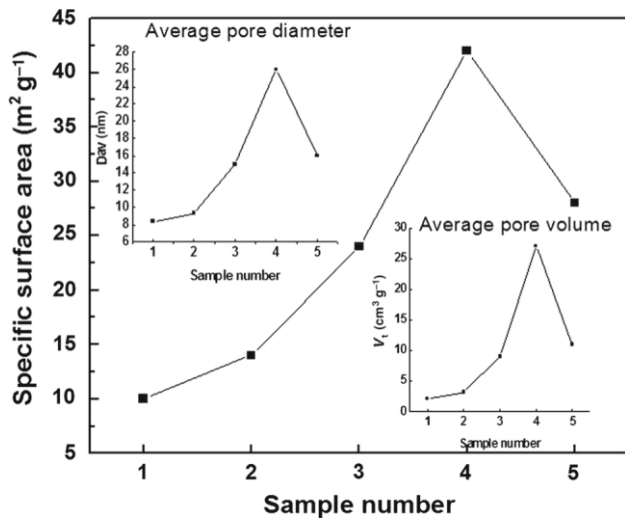
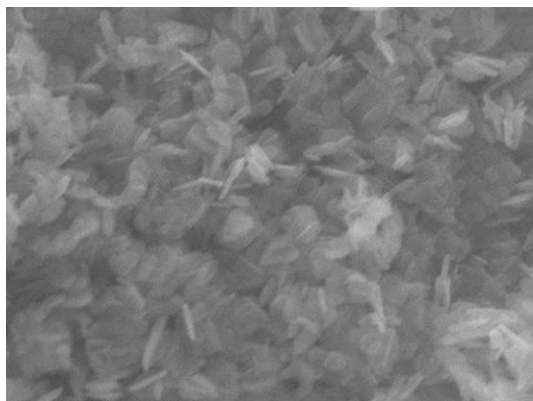
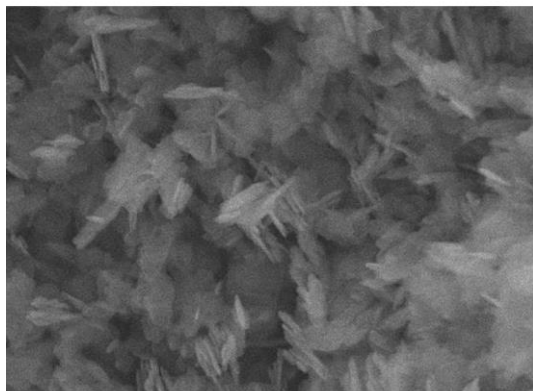


Figure 7. Specific surface areas, average pore volumes and average pore sizes of HT samples: (1) N0, (2) N1, (3) C0, (4) U0 and (5) U1.



SEM HV: 30.00 kV WD: 6.196 mm LYRA|TESCAN
 Vac: HiVac Det: SE
 SEM MAG: 50.00×kx Date (m/d/y): 12/10/15 Performance in nanospace

(a)



SEM HV: 30.00 kV WD: 5.835 mm LYRA|TESCAN
 Vac: HiVac Det: SE
 SEM MAG: 50.00×kx Date (m/d/y): 12/10/15 Performance in nanospace

(b)

Figure 8. SEM photograph of samples: (a) N0 and (b) N1.

The behavior of the N1 is quite different—the polymeric sample has higher specific surface area (higher precipitation rate at pH=13) as expected in advance from our previous studies [16,17]. The greatest share of mesopores and the largest average pore volumes are observed in the cases of zinc hydroxycarbonate intermediate phase (U0 and C0 samples)—figures 2, 3 and 4; hence, this is an alternative route to obtain the wurtzite phase—passing through zinc hydroxycarbonate intermediate phase. This phase is missing in the case of ZnO, obtained using NaOH as the precipitating agent (see figure 1). As far as the porosity is concerned, it is influenced to a great extent by possible gas evolution during the synthesis procedure. In our case we suppose CO₂ liberation in the case of ammonium hydroxycarbonate and urea precipitating agents —CO₂ is liberated as a result of thermal decomposition of the zinc hydroxycarbonate intermediate phase. In the case of C0 sample the decomposition of the zinc hydroxycarbonate intermediate phase proceeds at higher temperature (200°C) compared with the sample U0, which results in decrease of the specific surface area and lowering of the average pore volume. This is the explanation for the different texture of these two samples, both passing through the zinc hydroxycarbonate intermediate phase. It is worth noting that the different precipitants produce samples with different specific surface areas and morphology. The surface morphologies of ZnO samples prepared using NaOH as precipitant were investigated by SEM (figure 8a). The surface forms consisting of nano-sheets and nano-wires in sample N0 have lengths in the range of 250–500nm and diameters in the range of 30–60nm. When Pluronic was added into the solution, the surface morphology of the product was slightly changed—needle-shaped particles appeared having different lengths in the sample N1 (figure 8b), which are

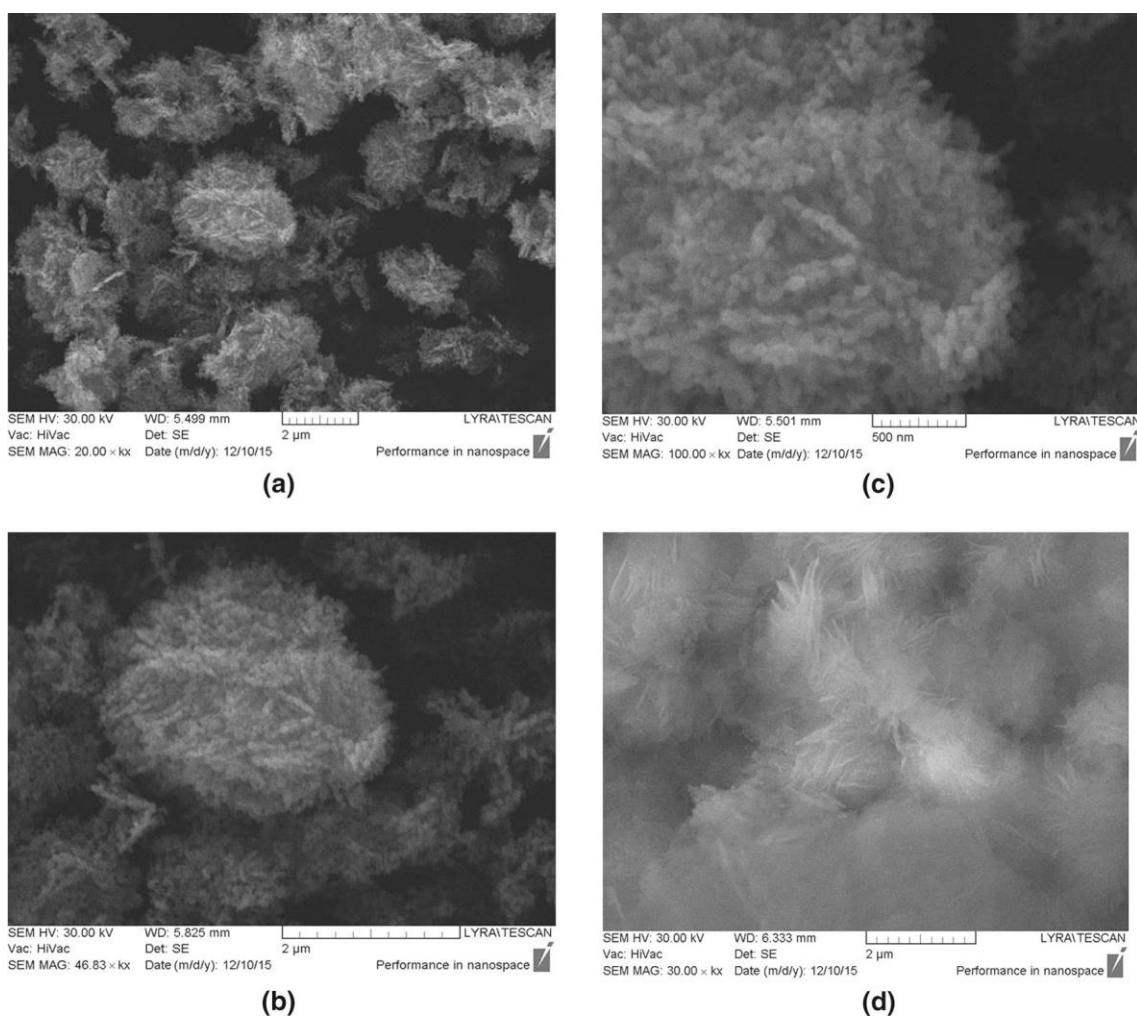


Figure 9. SEM photographs of sample: (a) C0, (b) C0, magnification 46,830, (c) C0, magnification 100,000 and (d) C1, magnification 18,000.

Similar to the structures of N0 sample. Similar elongated particles were also observed by Zhang and Mu [21] in HT-prepared ZnO powders. Due to the long PEO chains, the P123 micelles are large enough to act as nanoreactors in which the growth of larger particles is induced.

The surface morphology of the C0 sample reveals the existence of spherically shaped coral-like clusters, which consist of very small particles with average dimensions of 30–50nm (figure 9a and b). For example, figure 9c illustrates a higher magnification image of such spherical coral-like cluster. After the addition of P123 the clusters altered their shape. They have been transformed into finer grains, in which the individual particles are not distinguishable but on their surface many elongated needle-like particles have grown (figure 9d).

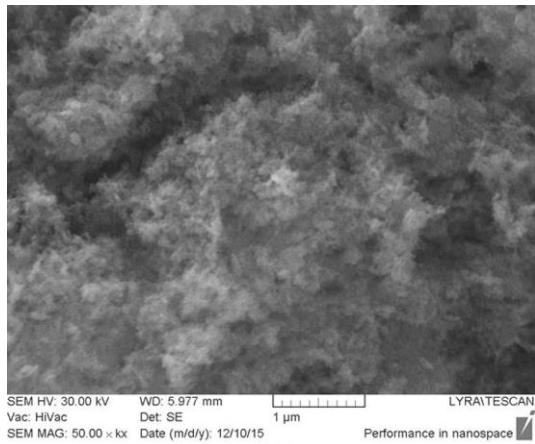
Figure 10a presents the surface morphology of a sample obtained by HT procedure using urea as the precipitant. The morphology is spongy-like formations with many pores, which are comparable to the pore size distribution in the sample U0 (figure 6). The surface morphology of sample U1 is quite different (figure 10b and c). It consists of many thin petals which contain elongated particles, similar in shape and size to particles on the surface of the samples N1 and C1.

3.2 EDX chemical analysis of U0 sample

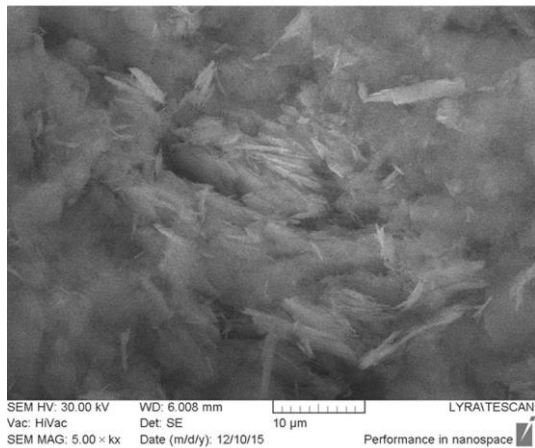
To establish the composition of the prepared products, EDX analyses were recorded. The typical EDX spectrum of sample U0 (figure 11) indicates the presence of both Zn and O peaks without any other elemental contamination. We have estimated the chemical composition in several points and the results confirmed that the quantities of O and Zn in all points are identical.

3.3 XPS data

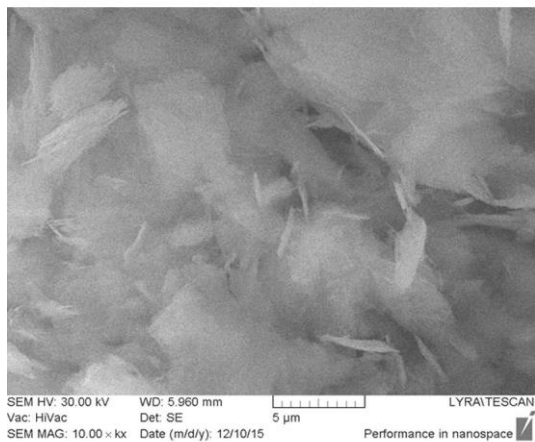
The O1s photoelectron lines were processed by an additional fitting procedure with XPSPEK41 software for the evaluation of different forms of oxygen. These results indicate that the chemical valence of Zn on the surface of the two studied



(a)



(b)



(c)

Figure 10. SEM photographs of sample: (a) U0, (b) U1, magnification 5000 and (c) U1, magnification 10,000.

Samples of ZnOis+2oxidationstate, with the binding energy value 1021.4eV of Zn2p_{3/2} peak (see figure 12). Simultaneously the difference between binding energies of the Zn2p_{1/2} and Zn2p_{3/2} signals is 23eV. The obtained results are in agreement with those already reported for ZnO [22–24].

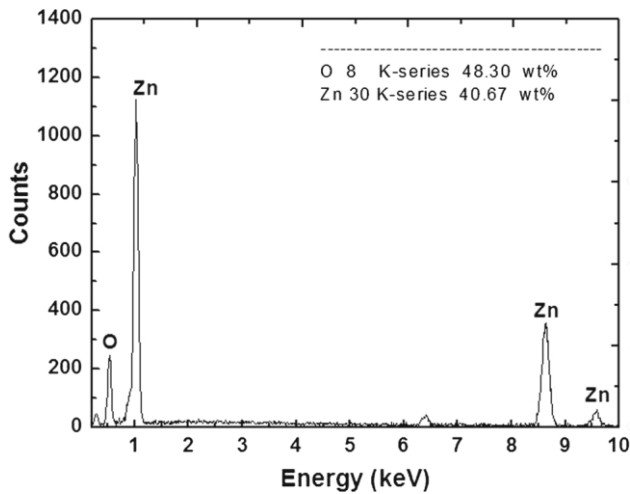


Figure 11. EDX analysis of U0 sample.

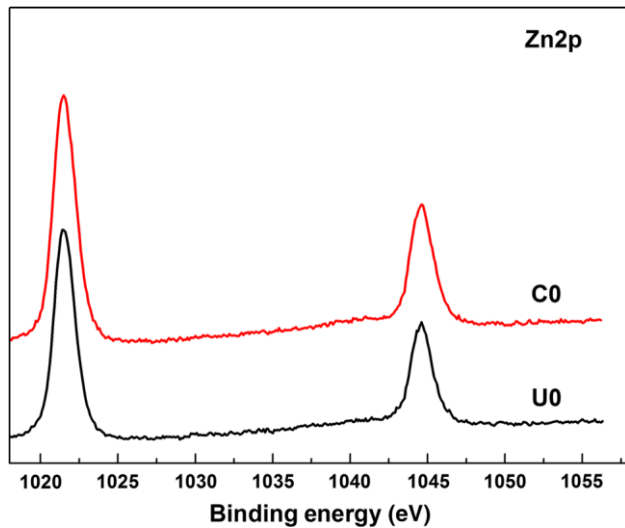


Figure 12. Zn2p core level spectra of samples C0 and U0.

The O1s photoelectron lines of C0 and U0 of ZnO powders, as mentioned earlier, were processed by a fitting procedure. The results from the fitting are represented in the next figure (figure 13a, b). The three peaks are clearly distinguishable. The first peak for both catalyst samples is associated with the O^{2-} ions in a highly ordered wurtzite structure of ZnO [22]. The first higher binding energy component at 531.2 eV is assigned to the oxygen-deficient region or oxygen vacancies within the ZnO matrix [25,26].

The 532.5 eV peak can be ascribed to the Zn–OH bonding and to the presence of another type of carbon–oxygen bonding, or other adsorbed molecules on the surface. This value is in agreement with the one already reported [27].

The calculated O/Zn atomic ratio is 1.22 for the C0 catalyst and 1.15 for the U0 one. This ratio shows that the U0 catalyst is closer to stoichiometricity compared with C0. This result is in coincidence with the XRD observation. We calculated the ratio of oxygen belonging to defects (oxygen vacancies) to the total oxygen content for the investigated catalysts as well as the ratio of oxygen associated with presence of hydroxyl groups, carbonate group or water on their surfaces. The C0 catalyst has larger number of defects; nevertheless, we observed with the U0 catalyst higher amount of oxygen related to existence of OH groups, other type of C–O bond or other adsorbed molecules on the surface. This correlates with the well-evolved surface and higher number of pores in it.

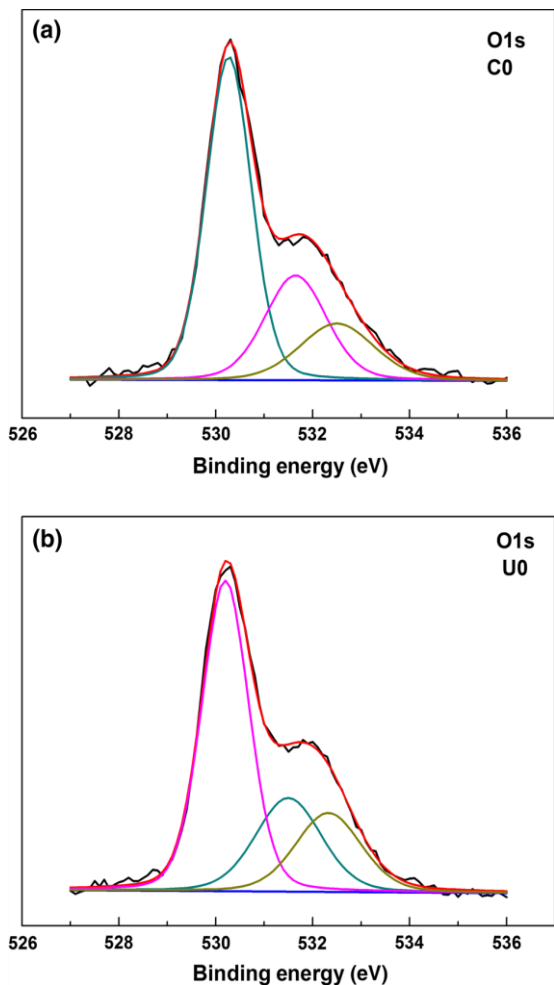


Figure 13. O1s core level spectra of samples: (a) C0 and (b) U0.

3.4 TG–DTA analyses

Figure 14 presents TG and DTA patterns of the U0 sample, dried at 120°C. An exothermic peak is observed at 170°C, interpreted as desorption of water molecules. At a higher temperature of 244°C an endothermic peak is registered, which corresponds to decomposition of zinc acetate precursor. Upon increasing the temperature further no other peaks are observed. The change in the TG curve indicates 22.5% mass loss of the sample. Similar results on thermal decomposition of zinc acetate and urea precursor have been obtained by Hu *et al* [28]. They observed an endothermic peak at 250°C with weight loss of about 25%.

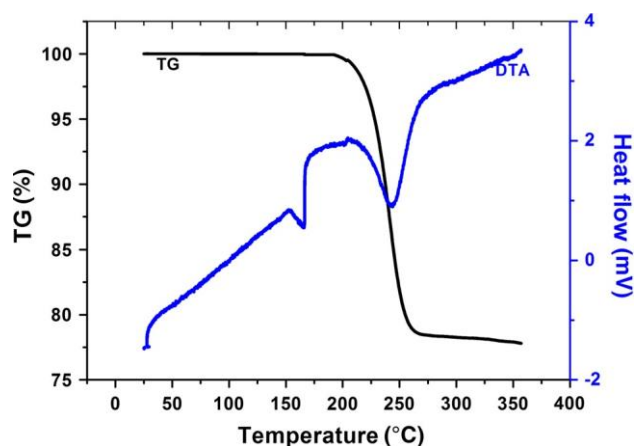


Figure 14. DTA–TG analyses of U0 sample, dried at 120°C .

3.5 DR UV–visible analyses

The bandgaps were estimated for each sample from its reflectance spectra. Performing Kubelka–Munk transformation of measured reflectance, the reflectance axis was converted. A tangent straight line is plotted on the generated curve; from the point where this line crosses the graph energy axis, the gap value is obtained (the figure is not presented here). The bandgap values of N0, C1 and U1 photocatalysts are 3.21eV. The photocatalyst N1 has bandgap value of 3.23eV, while for C0 and U0 this value is 3.24eV. The results show that the addition of P123 has no significant influence on the bandgap values.

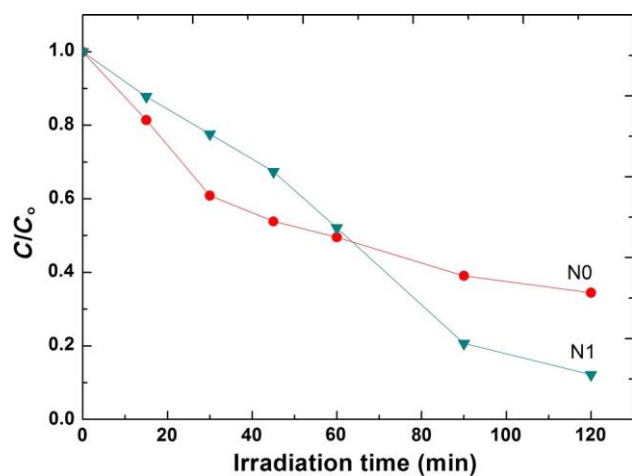


Figure 15. Kinetic curves of RB5 decolouration in coordinates $C/C_0 = f(t)$ for samples N0 and N1 at 20ppm initial dye concentration

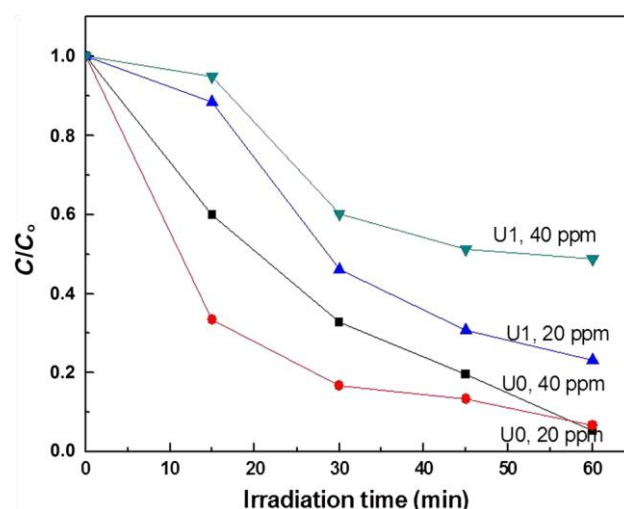


Figure 16. Kinetic curves of RB5 decolouration in coordinates $C/C_0 = f(t)$ for samples C0 and C1 at 20ppm initial dye concentration.

3.6 Photocatalytic activity tests

The photocatalytic efficiencies of the samples N0 and N1 were evaluated in the reaction of RB5 oxidative discoloration; the results are plotted in figure 15 as $C/C_0 = f(t)$, where C_0 and C are based on initial absorbance and current absorbance of the illuminated solution for time interval t , respectively. The experimental error is kept within the acceptable limit.

The reaction rate constant k was evaluated based on the slope of the $-\ln(C/C_0)$ vs. time of illumination straight line. The rate constant (k) for the N0 sample is $k = 0.82 \times 10^{-2} \text{ min}^{-1}$, while the N1 sample has a higher rate constant: $k = 1.73 \times 10^{-2} \text{ min}^{-1}$. Figure 16 presents the concentration decrease with the illumination time for samples produced by HT using ammonium hydroxycarbonate as precipitant. The experimental error is kept within the acceptable limit.

The C0 photocatalyst powder exhibits a complete decomposition of the dye within 120min under UV irradiation with a rate constant $k = 3.12 \times 10^{-2} \text{ min}^{-1}$, while sample C1.

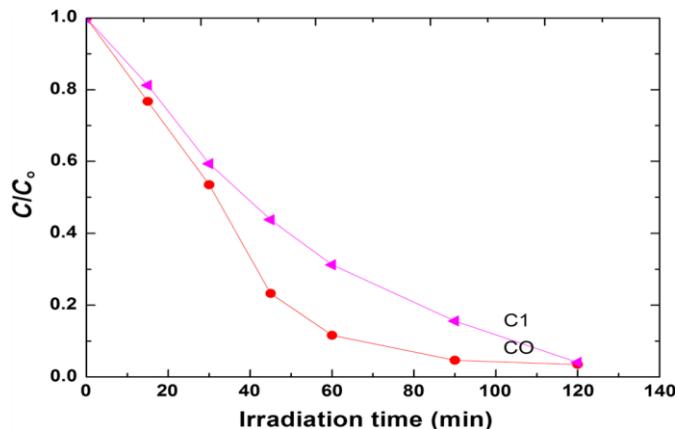


Figure 17. Kinetic curves of RB5 decoloration in coordinates $C/C_0 = f(t)$ for samples U0 and U1 at 20 and 40ppm initial dye concentration.

exhibits rate constant $k = 2.23 \times 10^{-2} \text{ min}^{-1}$. In this case the presence of polymer P123 plays a negative role in the activity of the samples probably due to the diffusion down the pores.

The photocatalytic efficiencies of the samples U0 and U1 were also evaluated in the reaction of RB5 oxidative discoloration for concentrations 20 and 40ppm and the results are plotted in figure 17. The adsorption of the 40ppm dye molecules on the surface lowers the formation rate of OH ions, decreases the number of catalytically active sites and consequently affects all the steps of the reaction, leading to a slightly lower photocatalytic reaction rate but even at 40ppm the sample U0 preserves the excellent photocatalytic performance.

The rate constants were calculated and they increased in the following order: $0.13 \times 10^{-2} \text{ min}^{-1} < 2.46 \times 10^{-2} \text{ min}^{-1} <$

$4.1 \times 10^{-2} \text{ min}^{-1} < 4.8 \times 10^{-2} \text{ min}^{-1}$ for samples U1 (40ppm), U0(40ppm), U1(20ppm) and U0(20ppm), respectively. This result confirms the most positive effect of use of urea as precipitant in the HT procedure on the photocatalytic properties of ZnO.

As proved by BET measurements the ZnO samples, produced by hydrothermal treatment of polymer-containing solution using NaOH, have slightly higher surface areas and possess greater share of mesopores than the reference sample N0. The presence of vesicles and needle-like particles reveals more internal surface area; therefore, the rate of dye molecules diffusion is increased, where upon the inner pores become easily accessible. This leads to higher rate of the photocatalytic reaction.

It is well known that the photocatalytic activities are higher in cases of larger specific surface areas of the photocatalysts as the reactant molecules are adsorbed on their surfaces. The larger surface area and larger pore volume of the polymermodified samples (N1) provide a larger number of active sites for the photocatalytic reactions. In addition to this, the mesoporous channels also facilitated the diffusion of large reactant molecules, thereby increasing the turnover number per active sites of photocatalytic material [29]. According to Baruah *et al*[30] the mesoporous structure of ZnO can provide more active sites available for adsorption of reactive species, due to the larger pore volume, which causes improvement in the photocatalytic activity due to better inner surface illumination. A similar conclusion about the roles of mesopores for effective adsorption of the pollutant on the catalyst resulting in relatively high photoactivity of TiO₂ photocatalyst has been proved in [31]. Additionally, the higher crystallinity degree of sample N1 decreases the bulk defects and lowers the recombination probability of photoexcited electrons and holes, which can enhance photocatalytic activity [32].

When ammonium hydroxycarbonate is applied as precipitant, the samples C0 and C1 possess higher surface area in comparison with N0 and N1 samples. The coral-like clusters consisting of very small particles ensure a larger number of active sites, which are responsible for the higher adsorption rate and rate of the photocatalytic reaction.

Urea-precipitated samples exhibit the best photocatalytic performance among the samples, which can be assigned to the largest specific surface area, largest pore volume and greater share of mesopores as well as the highest degree of crystallinity. This leads to enhanced adsorption of dye molecules, resulting in efficient photocatalytic degradation of dyes under irradiation. It has been reported for the case of OH groups on TiO₂ [33,34], that the higher surface concentration of OH groups is beneficial to photocatalytic activity—this is also valid in our case of ZnO photocatalyst [35]. The explanation is probably the adsorption

of RB5 molecule with its diazo group N=N, possessing pairs of non-bonded electrons, on the hydrogens of the polar OH groups.

4. Conclusions

The hydrothermal synthesis procedure involving urea and ammonium hydroxycarbonate as precipitants passes through zinc hydroxycarbonate intermediate during the synthesis, which is thermally decomposed into well-crystallized wurtzite ZnO phase after the thermal treatment. The best precipitating hydrothermal procedure to synthesize ZnO powders involves the use of urea as precipitating agent in the absence of Pluronic in view of the highest photocatalytic efficiency in the oxidative degradation of RB5. The most important promoting factors are the higher specific surface area, higher degree of crystallinity and greater share of mesopores in case of passing through zinc hydroxycarbonate intermediate phase for the samples, obtained using urea and ammonium hydroxycarbonate as precipitants. Probably the adsorption of RB5 molecule is involving the diazo group N=N, possessing pairs of non-bonded electrons, occur on the hydrogens of the polar OH groups, which is probably the explanation of the superior photocatalytic activity. The polymer exerts some beneficial effect only in the case of NaOH as precipitating agent.

Acknowledgements

We are grateful to EBR SANI for the financial support through the contract 'Development of advanced catalytic systems applicable to chemical and photochemical processes for neutralization of environmental pollutions'.

References

- [1] Sakthivel S, Neppolian B, Shankar M V, Arabindoo B, Palanichamy M and Murugesan V 2003 *Sol. Energy Mater. Sol. Cells* **77** 65
- [2] Kiomarsipour N, Razavi R S, Ghani K and Kioumarsipour M 2013 *Appl. Surf. Sci.* **270** 33
- [3] Stambolova I, Blaskov M, Shipochka M, Vassilev S, Dushkin C and Dimitriev Y 2010 *Mater. Chem. Phys.* **121** 447
- [4] de Lima J F, Martins R F and Serra O A *Opt. Mater.* **35** 56
- [5] Stambolova I, Blaskov V, Kaneva N, Shipochka M, Vassilev S, Dimitrov O *et al* 2014 *Mater. Sci. Semicond. Proc.* **25** 244
- [6] Suwanboon S and Amornpitoksuk P 2011 *Ceram. Int.* **37** 3515
- [7] Athma P V, Martinez A I, Johns N, Safeera T A, Reshmi R and Anila E I 2015 *Superlattices Microstruct.* **85** 379
- [8] Khalil M I, Al-Qunaibit M M, Al-zahem A M and Labis J P 2014 *Arab. J. Chem.* **7** 1178
- [9] Nishizawa H, Tani T and Matsuoka K 1984 *J. Am. Ceram. Soc.* **67** c98
- [10] Pudukudy M and Yaakob Z 2014 *Solid State Ion.* **30** 78 [11] Chen C C, Liu P and Lu C 2008 *Chem. Eng. J.* **144** 509
- [12] Zhang Y, Dai J Y, Ong H C, Wang N, Chan H L W and Choy C L 2004 *Chem. Phys. Lett.* **393** 17
- [13] Abdel Aal N, Al-Hazmi F, Al-Ghamdi A A, Al-Ghamdi A A, El-Tantawy F and Yakuphanoglu F 2015 *Spectrochim. Acta Part A* **135** 871
- [14] Wang J M and Gao L 2004 *Solid State Commun.* **132** 269 [15] Ni Y H, Wei X W, Hong J M and Ye Y 2005 *Mater. Sci. Eng. B* **121** 42
- [16] Eliyas A, Stambolova I, Blaskov V, Stoyanova D, Milenova K, Dimitrov L *et al* 2015 *Bulg. Chem. Commun.* **47** 94
- [17] Stambolova I, Blaskov V, Stoyanova D, Dimitrov L, Milenova K, Eliyas A *et al* 2015 *C. R. Acad. Bulg. Sci.* **68** 463
- [18] Hussain S, Liu T, Miao B, Kashif M, Aslam N, Rashad M *et al* 2015 *Ceram. Int.* **41** 4861
- [19] Liu I-H and Chen P 2010 *Ceram. Int.* **36** 1289
- [20] Miao Y, Zhang H, Yuan S, Jiao Z and Zhu X 2016 *J. Colloid Interface Sci.* **462** 9
- [21] Zhang Z and Mu J 2007 *J. Colloid Interface Sci.* **307** 79
- [22] Zheng J H, Jiang Q and Lian J S 2011 *Appl. Surf. Sci.* **257** 5083
- [23] Moulder J F, Stickle W F, Sobol P E and Bomben K D 1992 In *Handbook of X-ray photoelectron spectroscopy* J Chastain (ed) (Eden Prairie: Perkin-Elmer Corporation) p 89
- [24] Das J, Pradhan SK, Sahu DR, Mishra DK, Sarangi SN, Nayak B B *et al* 2010 *Phys. B* **405** 2492
- [25] Wang H H and Xie C S 2008 *Phys. E* **40** 2724
- [26] Wang H H, Baek S H, Song J J, Lee J H and Lim S W 2008

Nanotechnology **19** art. no. 075607

- [27] Al-Gaashani R, Radiman S, Daud A R, Tabet N and Al-Douri Y 2013 *Ceram. Int.* **39** 2283
- [28] Hu S-H, Chen Y-C, Hwang C-C, Peng C-H and Gong D-C 2010 *J. Mater. Sci.* **45** 5309
- [29] Lamba R, Umar A, Mehta S K and Kansal S K 2015 *Talanta* **131** 490
- [30] Baruah S, Mahmood M A, Myint M I Z, Bora T and Dutta J 2010 *Beilstein J. Nanotechnol.* **1** 14
- [31] Bacsa R R and Kiwi J 1998 *Appl. Catal. B* **16** 19
- [32] Li D and Haneda H 2003 *Chemosphere* **51** 129
- [33] Yu J C, Yu J and Zhao J 2002 *Appl. Catal. B Environ.* **36** 31
- [34] Hoffmann M R, Martin S T, Choi W and Bahnemann D 1995 *Chem. Rev.* **95** 69
- [35] Yang C, Li Q, Tang L, Xin K, Bai A and Yu Y 2015 *Appl. Surf. Sci.* **357** 1928